UNIVERSITY OF CALIFORIA,
IRVINE

Patient-specific optimization of automated detection improves seizure onset zone localization based on high frequency oscillations

THESIS

submitted in partial satisfaction of the requirements for the degree of

MASTER OF SCIENCE
in Biomedical Engineering

by

Casey Trevino

Thesis Committee:
Assistant Professor Beth Lopour, Chair
Professor Frithjof Kruggel
Dr. Jack Lin

2020

Table of Contents

List of Figures

List of Tables

Acknowledgements

Firstly, I want to express my profound gratitude to my advisor, Dr. Beth Lopour, who has served as my professor and mentor during my studies at UCI. She is knowledgeable, kind, and dedicated to her students, and I am grateful to have had her support and encouragement throughout my graduate education. Without her guidance and diligence, this project would not be what it is today.

Secondly, I would like recognize the invaluable contributions from my thesis committee, Dr. Frithjoff Kruggel and Dr. Jack Lin. Dr. Lin provided insightful commentary and essential clinical data, aiding in the realization of this project. As my professor, Dr. Kruggel taught important concepts in his lectures which I applied to this project and will continue to use in my career.

Thirdly, I want to thank my lab mates for their encouragement, advice, and support. To Krit, thank you for sharing your knowledge, resources, and advice during the beginning development of this project which helped me lay the foundation for this work. To Derek, thank you for always helping me when I felt stuck and for your endless inspiration and advice. To Sara and Kavya, thank you for being my classmates and for sharing your resources and experiences with me. And to Trisha, thank you for your encouragement and positivity, especially during the difficult situations that arose.

Lastly, I want to acknowledge my friends and family who have always supported and encouraged me in all my endeavors.

Abstract of Thesis

Patient-specific optimization of automated detection improves seizure onset zone localization based on high frequency oscillations

by

Casey Trevino

Master of Science in Biomedical Engineering

University of California, Irvine, 2020

Professor Beth Lopour, Chair

High frequency oscillations (HFOs) are a promising new biomarker of epileptogenicity, as they occur more frequently in the seizure onset zone (SOZ) and may aid in the demarcation of the epileptogentic zone. Development of reliable, automatic HFO detection algorithms is necessary for translation into clinical practice. While existing algorithms have demonstrated sufficient levels of sensitivity and specificity on individual data sets, there are currently no standards for their broad application. It is not uncommon for a previously validated algorithm to work poorly when applied to a new data set, and there is no consensus on whether (and how) parameter optimization should be done. Here we evaluate the impact of detector optimization on two independent datasets, consisting of twenty medically refractory epilepsy patients with seizure free surgical outcomes, using a widely cited automatic HFO detector based on the root-mean-square amplitude. We calculated SOZ localization results over a wide range of detection parameters and assessed the variance in results across patients. The optimal parameters were

patient-specific, and in some cases, the most accurate localization resulted from detection with unconventional parameters. This suggests that the standard configurations are not suited for all patients. To overcome this obstacle, we suggest a novel method of coalescing the results from multiple parameter sets to isolate robust HFOs of epileptic tissue. This method resulted in localization accuracy that was comparable to the optimal parameter sets, without the difficult task of choosing a single parameter set to rely on. This work has the potential to eliminate per-patient optimization of HFO detection, which will support translation into clinical practice, and it suggests that future studies should continue investigating ways to address patient variability before applying automatic detection algorithms.

1. Introduction

1.1. Electrophysiological markers of the seizure onset zone

Epilepsy is a neurological disorder characterized by the occurrence of spontaneous, unpredictable seizures which affects approximately 1% of the world's population (Ramey et al., 2013). Epilepsy is commonly treated with medication, however approximately 30% of patients are unable to achieve adequate seizure control using medication alone (Kwan & Brodie, 2000). For such patients with medically refractory epilepsy, surgical resection of neural tissue associated with seizure generation offers a viable solution to eliminate or significantly reduce the occurrence of seizures (Schuele & Lüders, 2008).

Successful surgical treatment depends upon the identification of the epileptogenic zone (EZ), a theoretical construct defined as all brain areas potentially able to generate seizures (Jacobs et al., 2012). In current clinical practice, patients undergo pre-surgical evaluation in which intracranial electrodes are implanted and used to monitor seizure activity. The goal of this procedure is to identify the seizure onset zone (SOZ), which remains the best proxy for the EZ. The SOZ is defined as the area in which clinical seizures start based on direct electrophysiological measurements during pre-surgical evaluation (Rosenow & Lüders, 2001). Clinicians identify the SOZ through intensive visual analysis of intracranial electroencephalography (iEEG) and monitor for areas characterized by increased epileptiform discharges. Also called epileptic "spikes," these discharges are caused by synchronous bursts of neuronal activity. Epileptiform discharges are considered indicative of the SOZ due to their high degree of association with seizures (Westmoreland, 1996). However, it has also been found that epileptiform discharges occur outside the SOZ (Bautista et al., 1999). Furthermore, patients with

spikes occurring in multiple brain areas are less likely to become seizure free after surgery than patients with well localized spikes (Bautista et al., 1999). Consequently, only 50-60% of patients are seizure free following resective surgery, emphasizing the need to improve localization of the EZ (Edelvik et al., 2013).

Over the past two decades, there has been growing interest in analyzing activity above the gamma band (40-100Hz) in the form of electrographic events called high-frequency oscillations (HFOs). HFOs have been shown to provide more accurate localization of the EZ than spikes (Jacobs et al., 2010). They are generally defined as spontaneous EEG patterns that consist of at least four oscillations with frequency > 100 Hz that clearly stand out from the background activity (Bragin et al., 1999). HFOs are often further divided into "ripples" in the 80-250 Hz band and "fast ripples" in the 250-500 Hz frequency range. Since their discovery in rodent models, numerous studies have demonstrated the ability to record HFOs in humans using clinical macro electrodes (Crépon et al., 2010; Worrell et al., 2008). Furthermore, HFOs occur during the interictal period, reducing risk and discomfort for patients by minimizing recording time and the necessity of ictal recordings (Migliorelli et al., 2017). Interictal HFOs are a promising biomarker for the SOZ, as they occur more frequently at the site of seizure onset (Jacobs et al., 2012; Zijlmans et al., 2012). It has also been suggested that HFOs are more specific to the SOZ than spikes (Crépon et al., 2010; Jacobs et al., 2008; Staba & Bragin, 2011), although another study found that their co-occurrence with spikes was the best predictor of the SOZ (Roehri et al., 2018). The removal of HFO-generating regions has also been correlated with good post-surgical outcome (Akiyama et al., 2011; Jacobs et al., 2010; Wu et al., 2010). Moreover, it was demonstrated that HFOs are not specific to brain lesions, further strengthening

its case as a marker of epileptogenic tissue rather than other pathologic tissue changes (Jacobs et al., 2009).

1.2. Automatic HFO detection

HFOs are conventionally detected through visual identification by expert reviewers, and this is currently accepted as the gold standard (Ferrari-Marinho et al., 2015; Jacobs et al., 2014); however, visual marking is time-consuming, subjective, and non-reproducible (Zelmann et al., 2012). Several automated HFO detection algorithms have been developed to facilitate HFO analysis. The development of automatic HFO detectors is significant due to its elimination of reviewer bias, efficiency, reproducibility, and standardization in defining clinically relevant HFOs compared to conventional visual identification. Furthermore, translating HFO analysis into clinical practice cannot be accomplished without automated methods (Worrell et al., 2012)

The first automatic HFO detector was developed to identify HFOs in hippocampal microelectrode recordings from humans and rats (Staba et al., 2002). Briefly, the algorithm identified time periods in which the signal energy of the band pass filtered data (100-500 Hz) exceeded a threshold for at least three oscillations (3 cycles), using the signal's root-mean-square (RMS) amplitude to estimate energy. We will refer to this as the RMS detector. This algorithm generally achieves high sensitivity compared to visual markings, but it does so at the expense of high false positive rates (Gardner et al., 2007).

Subsequent development of automatic HFO detectors included other measures of signal energy, frequency analysis, and machine learning techniques (Navarrete et al., 2016). Many of these detectors were influenced by the RMS detector, either stemming from the detection

algorithm, building upon the algorithm, or benchmarking against it as the gold standard (Blanco et al., 2010; Burnos et al., 2014; Chaibi et al., 2013; Gliske et al., 2016; Wu et al., 2018; Zelmann et al., 2010). For example, the line-length detector replaced the short-time energy estimate with line length and reported improved sensitivity and specificity values benchmarked against the RMS detector for their analysis in clinical EEG data (0.1-100Hz) (Gardner et al., 2007). Blanco et al. (2010) utilized the RMS detector for the first stage of initial detection before using data mining to classify the remaining HFOs. A more recent detector used a fuzzy-c-means (FCM)- quantization error modeling (QEM)-based expectation maximization (EM) - Gaussian mixture modeling (GMM) algorithm to analyze significant features from HFOs detected by the RMS detector, as a way to isolate artifacts (Wu et al., 2018).

When new automatic HFO detection algorithms are proposed, they are generally developed for detection in a specific frequency band, location of the brain, and/or electrodes types (Zelmann et al., 2012). When these algorithms are subsequently applied to a new dataset, it can be preferable to use the published configuration, in order to provide independent validation of the algorithm's utility, promote reproducibility of results, and to avoid overfitting to the data. Moreover, optimization procedures are often complex and not feasible in a clinical setting. However, the use of standard configurations can lead to suboptimal performance when used for a different data set, frequency range, or detection task. For example, when new algorithms are directly compared to previously published algorithms, without optimizing the parameters, the results tend to be worse than originally reported (Burnos et al., 2014; Gardner et al., 2007; Wu et al., 2018; Zelmann et al., 2012). This suggests that optimization may be an important step of HFO detection, which is supported by studies noting that optimizing detection parameters can improve sensitivity (Zelmann et al., 2012) and localization accuracy (Chaibi et al., 2013;

Charupanit & Lopour, 2017; Dümpelmann et al., 2012). However, the optimization procedures in these studies were often limited to small parameter ranges, performed only to compare performance across detectors, and did not account for patient variability. Thus, it remains unknown whether patient-specific optimization is necessary, which parameter ranges are relevant for HFOs, and how this optimization should be accomplished.

1.3. Motivation

In the present study, we evaluated the significance of optimization for automatic HFO detection using two independent datasets. Using a frequently cited automatic detector, we tested a wide range of algorithm parameter sets and determined the SOZ localization accuracy for each one. Our goal was to determine optimal parameter ranges for HFO detection, assess the variation in results across patients, and investigate the impact of optimization on the accuracy of SOZ localization. Moreover, we aimed to use these results to suggest a standardized and simplified optimization procedure.

2. Methods

2.1. Clinical data collection

Twenty patients with medically refractory epilepsy from two medical centers were identified retrospectively and included in this study. Seven of these patients underwent implantation of intracranial electrodes for presurgical evaluation from June 2015 to March 2017 at the University of California, Irvine (UCI) Medical Center. We will refer to this as the UCI dataset. These patients had postoperative outcome of Engel Class I, which indicates that the patient was seizure free following resective surgery. This suggests that the clinical SOZ localization was successful. If patients had multiple seizures with different regions of onset during recording, all SOZ channels were considered SOZ. The demographic and clinical characteristics of these subjects are shown in Table 1. Collection and analysis of retrospective patient data for this study was approved by the Institutional Review Board of the University of California, Irvine.

Table 1. Patient demographics of the UCI dataset. Abbreviations: AM = amygdala; AH = anterior hippocampus; depth = depth electrode; FLE = frontal lobe epilepsy; grid = grid electrode; HH = head of hippocampus; HP = hippocampus; L = left; MF = mesial frontal; PFC = pre-frontal cortex; TH = tail of hippocampus; TLE = temporal lobe epilepsy; R = right

Subject	Age, Gender	Seizure semiology	MRI	Diagnosis	Electrodes	SOZ channels	Surgery	Engel outcome	Postoperative follow-up (months)
1	44, M	Unknown	Cortical Dysplasia in PFC	FLE	1 grid 8x8 2 grid 2x8 1 grid 4x8	RMF28-32	R Frontal Lobectomy	IA	47
2	50, M	Unknown	White matter changes in frontal lobe; possible right mesial temporal atrophy	TLE	5 depth 1x16	RAH5-8	R Temporal Lobectomy	IB	22
3	46, M	Complex Partial Seizures	Right Hippocampal Sclerosis	TLE	5 depth 1x16	RAH4	R Temporal Lobectomy	IA	41
4	34, M	Complex Partial Seizures	Bilateral hypometabolism and hippocampus abnormalities; mild left atrophy	TLE	2 depth (1x14) 3 depth (1x16) 2 grid (2x6) 1 depth (1x10)	RAM1-2, RHP1-3	R Temporal Lobectomy	IA	2
5	57, F	Complex Partial (Focal Dyscognitive) Seizures	None	TLE	11 depth (1x10) 1 depth (1x12)	LHH1-3, LTH2-3	L Lateral Temporal Lobectomy, L Amygdala and Hippocampal Resection	IA	23
6	53, F	Complex Partial Seizures	Left Mesial Temporal Sclerosis	TLE	10 depth (1x10)	LTH1	L Temporal Lobectomy	IA	32
7	54, F	Complex Partial Seizures	None	TLE	10 depth, (1x10)	RHH1-4, RAM1-2	R Temporal Lobectomy	IB	26

The remaining thirteen patients included in this study were obtained from a freely available online database provided by Fedele et al. (2017) at iEEG.org (http://crcns.org/data-sets/methods/ieeg-1/about-ieeg-1). These patients underwent invasive EEG recordings with subdural and/or depth electrodes from March 2012 to April 2016 at the University Hospital Zurich as part of their presurgical evaluation. We refer to these thirteen patients as the ETH Zurich dataset. As in the UCI dataset, the included patients reported good clinical outcomes (class 1) assigned at least 1 year following resective surgery based on the International League Against Epilepsy (ILAE) scale. Information regarding electrode types, data acquisition, and sleep scoring can be found in Fedele et al. (2017). Patient demographics for the ETH Zurich dataset are in Table 2.

Table 2. Patient demographics of the ETH Zurich dataset. Abbreviations: depth = depth electrode; ETE = extratemporal epilepsy; ILAE = International League Against Epilepsy; Les = lesionectomy; sAHE = selective amygdala hippocampectomy; strip = strip electrode; TLE = temporal lobe epilepsy

Subject	Age, Gender	Epilepsy	Type of electrodes	Channels in resected tissue	Surgery	ILAE outcome	Postoperative follow-up (months)
8	25, M	TLE	5 depth 1 strip 4 x 1 1 strip 6 x 1	AHR1-2, AHR2-3, AHR3-4, AR1-2, AR2-3, AR3-4, PHR1-2, PHR2-3, PHR3-4	sAHE; Les	1	12
9	33, M	TLE	8 depth	AR1-2, AR2-3, AR3-4, ER1-2, ER2-3, ER3-4, HR1-2, HR2-3, HR3-4, PR1-2, PR2-3, PR3-4	sAHE; Les	1	29
10	20, F	TLE	5 depth	AHL1-2, AHL2-3, AHL3-4, AL1-2, AL2-3, AL3-4, ECL1-2, ECL2-3, ECL3-4, PHL1-2, PHL2-3, PHL3-4	sAHE	1	13
11	20, F	TLE	8 depth	AR1-2, AR2-3, AR3-4, ER1-2, ER2-3, ER3-4, HR1-2, HR2-3, HR3-4, PR1-2, PR2-3, PR3-4	sAHE	1	41
12	40, M	TLE	8 depth	AR1-2, AR2-3, AR3-4, ER1-2, ER2-3, ER3-4, HR1-2, HR2-3, HR3-4, PR1-2, PR2-3, PR3-4	sAHE	1	14
13	48, M	TLE	8 depth	AR1-2, AR2-3, AR3-4, ER1-2, ER2-3, ER3-4, HR1-2, HR2-3, HR3-4, PR1-2, PR2-3, PR3-4	sAHE	1	11
14	37, M	ETE	1 grid 8 x 4 2 strips 4 x 1	IPR1-2, IPR2-3, IPR3-4	Les	1	36
15	36, M	ETE	1 grid 8 x 8 1 depth	TR1-2, TR2-3, TR3-4	Les	1	37
16	49, M	ETE	1 grid 8 x 4 1 depth	GL1-2, GL2-3, GL9-10, GL10-11, GL11-12, GL12-13, GL17-18, GL18-19, GL19-20, GL20-21, GL21-22, GL25-26, GL26-27, GL27-28, GL28-29, GL29-30, GL30-31, GL31-32, TL1-2, TL2-3, TL3-4	Les	1	25
17	17, M	ETE	1 grid 8 x 8 1 depth	TR1-2, TR2-3, TR3-4	Les	1	25
18	46, F	ETE	2 grids 8 x 2 1 strip 6 x 1 1 strip 4 x 1 1 depth	IPR3-4	Les	1	10
19	31, F	ETE	1 grid 8 x 4 2 strips 4 x 1	TBAL2-3, TBAL3-4, TLL1-2, TLL9-10	Les	1	25
20	17, F	ETE	1 grid 8 x 4 1 depth	TL1-2, TL2-3, TL3-4	Les	1	19

2.2. Data acquisition

Intracranial EEG was recorded for each patient using a combination of subdural electrocorticogram (ECoG) grids and strips, as well as depth electrodes. Recordings from the UCI dataset were collected using a Nihon Kohden JE-120A amplifier with a minimum sampling frequency of 2000 Hz for all patients. Recorded data were re-referenced to a bipolar montage for

analysis to support precise localization. All bipolar re-referenced channel pairs that included an SOZ channel were deemed as SOZ (for example, channels RAH3-4 and RAH4-5 of UCI patient 3 were considered SOZ). Five 3-minute epochs from one night of iEEG recording were randomly selected for each UCI patient, for a total of 15 minutes per patient. Each epoch was chosen from data recorded between 8pm and 8am to improve the likelihood of analyzing sleep data, as HFO rates increase during slow-wave sleep compared to wakefulness (Bagshaw et al., 2009; Clemens et al., 2003; Staba et al., 2004) and the occurrence of muscle artifacts is reduced. All epochs consisted of interictal data, recorded at least 1 hour away from seizure activity to reduce the influence of seizures on HFOs (Pearce et al., 2013). We analyzed all implanted electrodes, which ranged from 80 to 128 total electrodes for each UCI patient.

All interictal recordings from the ETH Zurich dataset were obtained at least 3 hours away from seizure activity, and we analyzed five 5-minute epochs of slow wave sleep from one night of recording. We included the same channels used for analysis by the original authors; the included and excluded channels can be found in the supplementary information provided by Fedele et al. (2017). Of note, the number of analyzed channels for each patient ranged from 15 to 53. For patients implanted with depth electrodes, superficial contacts (>7) were excluded from analysis. For the analysis in the current study, we will define the "SOZ channels" to be the bipolar re-referenced channels within the resected area for each patient; the specific sites of seizure onset within the resected area were not provided.

2.3. Data processing

2.3.1 Automatic HFO detection

Automated HFO detection was performed using the RMS detector introduced by Staba et al. (2002). We used the RMS detector because it is referenced often as a benchmark for new algorithms, serves as the core of many other detectors, and is algorithmically simple to implement and examine. In this algorithm, broadband data is bandpass filtered in the 100-500Hz frequency range, and candidate events are identified when the RMS of the bandpass filtered signal exceeds a threshold for a minimum duration (thldt) (Figure 1A). The RMS signal is

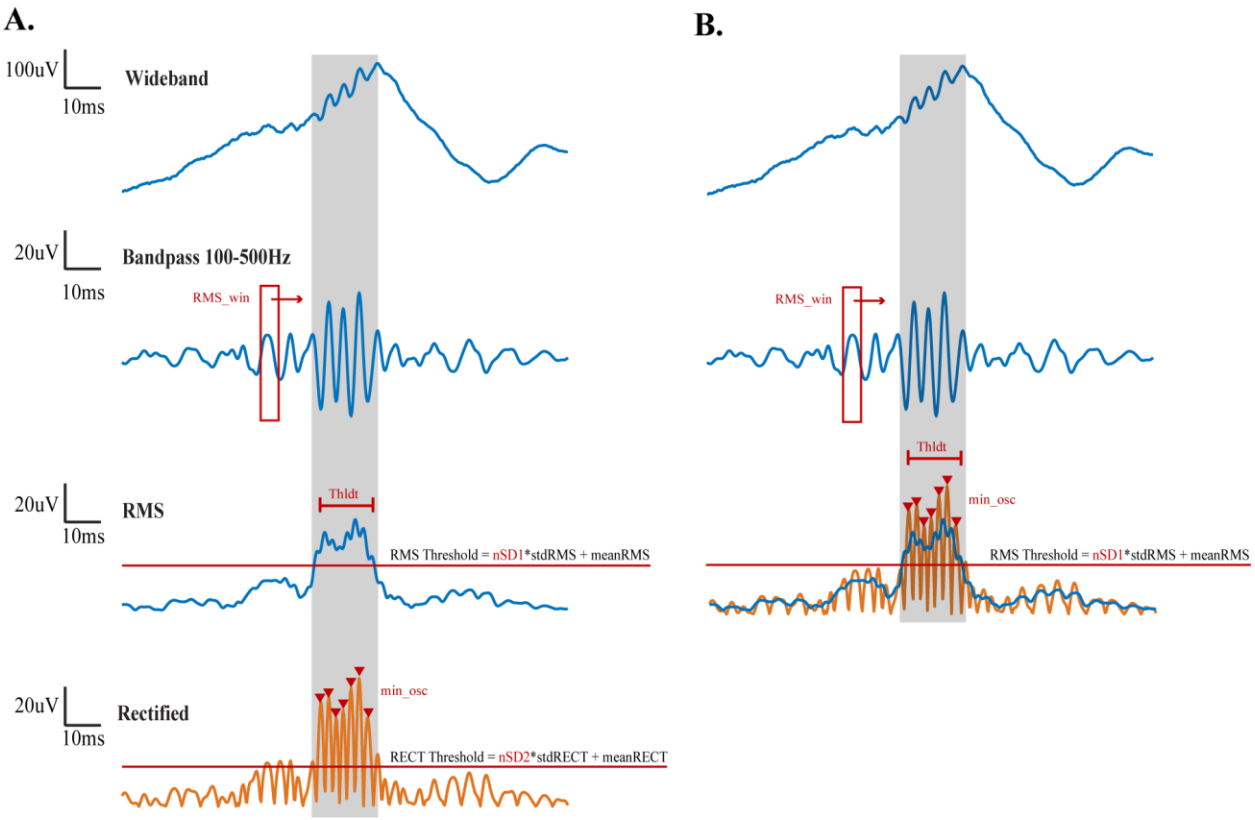

Figure 1. Automatic HFO detection algorithm. (A) Full RMS Detector (B) Reduced RMS Detector. The shaded gray region represents the window containing the identified candidate event.

calculated using a moving window (RMS_win), and the first threshold is defined as five standard deviations (nSD1) above the mean RMS signal. Consecutive events separated by less than a predefined gap time (tstep) are combined into one event. Candidate events are retained when a minimum number of peaks (min_osc) in the rectified filtered data exceed a second threshold defined as 3 standard deviations (nSD2) above the mean rectified data.

To reduce algorithmic complexity and minimize the number of optimization parameters, we simplified the RMS detector algorithm by modifying the threshold applied to the rectified data (Figure 1B). We set threshold two equal to threshold one, as they both ensure that the signal's energy exceeds a threshold determined from baseline activity. As in the original algorithm, we required that a minimum number of peaks in the rectified filtered data exceed this threshold, to promote rejection of fast transients. All other steps in the original algorithm were maintained.

The algorithm used in our analysis thus contains five parameters that must be considered during optimization: RMS window size (rms_win), minimum event duration (thldt), number of standard deviations above the mean RMS signal (nSD1), minimum gap time (tstep), and minimum number of oscillations (min_osc). From these parameters, we varied the three that directly affect initial detection of candidate events: RMS window size, minimum event duration, and threshold. Because the minimum gap time is a post-processing step to join candidate events and the minimum number of oscillations has little impact as a criterion due to the redundancy with minimum event duration, we kept these variables constant at their default values. The default values of each parameter and values tested during the optimization procedure are described in Table 3.

Table 3. Detection parameters varied during optimization and corresponding ranges of values. Default values are in red. The default value for minimum gap time is 10ms and minimum number of oscillations is 6.

Threshold (nSD1)	1, 2, 3, 4, 5, 6, 7, 8, 9, 10, 11, 12, 13, 14, 15
RMS window size (RMS win) (ms)	2, 3, 5, 7, 9, 11, 15, 17, 20
Minimum event duration (thldt) (ms)	6, 12

2.3.2 Automatic artifact rejection

Because the RMS detector is highly sensitive, we implemented two artifact rejection methods to improve specificity: PopDet and BkgStabaDet. Both methods were introduced by Gliske et al. (2016) for the purpose of creating a generalized HFO detection algorithm for long term intracranial EEG recordings, such that the algorithm automatically identifies quality HFOs without any patient-specific tuning or operator intervention (Gliske et al., 2016). These artifact rejection steps were designed using the RMS detector for initial detection, making them appropriate for our analysis. In this study, the default parameters from Gliske et al. (2016) were used for all subjects and all parameter sets.

2.3.2.1 PopDet

The popDet criterion was designed to detect DC shifts and fast transients commonly found in EEG data (Figure 2A, B). When a DC shift or fast transient is filtered, it can have the appearance of an HFO in the 100-500 Hz frequency band (Bénar et al., 2010; Zelmann et al., 2010). However, these transients also contain power at very high frequencies, whereas a true HFO should have band-limited power. Therefore, the popDet identifies instances when the line length of a 0.1s window in the 850-990 Hz frequency range exceeds a threshold of 5 standard

deviations above the mean line length calculated from baseline. Baseline is defined as a 5-second window preceding the window being evaluated.

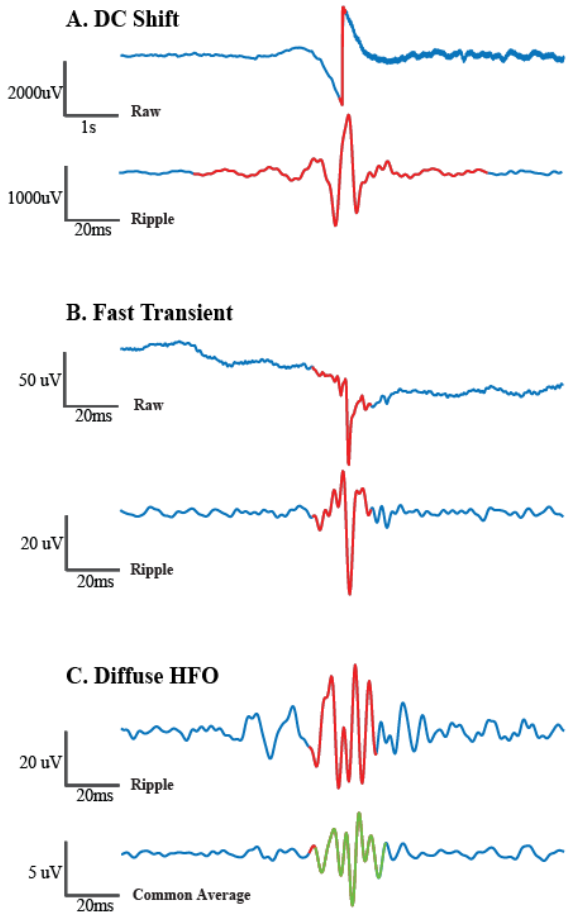

Figure 2. Examples of rejected artifacts. Both broadband (A, B, top) and bandpass filtered data (A, B, bottom) are shown for A and B. Bandpass filtered data from one channel (C, top) and the common average bandpass filtered data (C, bottom) are shown in C. (A) DC Shift detected by popDet and (B) fast transient detected by popDet, with the artifacts highlighted in red. (C) Diffuse HFO detected by BkgStabaDet. The candidate HFO detected on the common average (highlighted in green) represents the common average HFO that occurred at or near (±100ms) the same time as the detected HFO (highlighted in red) in the bandpass filtered signal.

2.3.2.2 BkgStabaDet

The BkgStabaDet was designed to detect diffuse HFOs, which are considered artifacts because they contradict the idea that HFOs should be focal events (Bragin et al., 2002, 2011). If an HFO occurs in all channels of a depth electrode or grid, it will appear in the common average (Figure 2C). Therefore, if an HFO is detected in the common average signal, we considered it to be artifact. As in the Gliske et al. (2016) implementation, we applied the RMS detector from Staba et al. (2002) to the common average using the default parameters. Detections in a single channel that occurred within 100ms of detections in the common average were marked as artifacts.

2.4 Data analysis

2.4.1 SOZ localization defined by rate thresholding

After HFO detection and artifact rejection were performed for a given parameter set, the HFO rate for each channel was averaged across epochs. To localize the SOZ, a threshold was applied to the average HFO rates to classify channels as in the SOZ and outside the SOZ (nSOZ). Channels with average HFO rates exceeding the rate threshold were classified as SOZ and the remaining channels were classified as nSOZ.

2.4.2 Receiver operator characteristic curves and precision-recall curves

For each parameter set, we used a receiver operator characteristic (ROC) curve to characterize the ability of automatic HFO detection to localize the SOZ. For channels defined

clinically as SOZ (based on visual interpretation of ictal iEEG), channels automatically classified as SOZ were marked as true positives (TP) and those automatically classified as nSOZ were marked as false negatives (FN). For channels defined clinically as nSOZ, the channels automatically classified as nSOZ were marked as true negatives (TN) and those classified as SOZ were marked as false positives (FP). The ROC curve was plotted by varying the rate threshold and determining the true positive rate (TPR) and false positive rate (FPR) for each value:

$$\mathrm{TPR} = \frac{\mathrm{TP}}{\mathrm{TP+FN}} \qquad (1)$$

$$\mathrm{FPR} = \frac{\mathrm{FP}}{\mathrm{FP+TN}} \qquad (2)$$

The area under the ROC curve (AUC) was determined for each parameter set for all patients.

As a complementary measure, Precision-Recall (PR) scores were evaluated to examine the positive predictive value for each parameter set. Precision-Recall analyses are preferred when prediction power of imbalanced classes is being evaluated; in our case, we have imbalanced classes represented by the small subset of SOZ channels compared to the larger class of nSOZ channels for UCI patients, and the small subset of nSOZ channels compared to the larger class of SOZ channels for some ETH Zurich patients (specifically, patients 10 and 16). Precision (P), Recall (R), and the F1 score (F1) are computed as follows:

$$\mathrm{P} = \frac{\mathrm{TP}}{\mathrm{TP+FP}} \qquad (3)$$

$$\mathrm{R} = \frac{\mathrm{TP}}{\mathrm{TP+FN}} \qquad (4)$$

$$\mathrm{F1} = 2\,\frac{\mathrm{P*R}}{\mathrm{P+R}} \qquad (5)$$

Like the ROC curve, the PR curve was constructed by varying the rate threshold and calculating the precision, recall, and F1 score for each value. The optimal F1 score was defined as its maximum value, which represents the maximum harmonic mean of precision and recall.

After calculating the ROC and PR results for each parameter set, the maximum AUC of the ROC curve, as well as the optimal F1 score of the PR curve were determined for each patient.

2.4.3 Artifact counting

To assess the impact of the automated artifact rejection steps, we calculated the percentage of candidate HFOs rejected for each parameter set. The percentage of rejected artifacts by popDet was calculated as the total number of artifacts marked by popDet over the total number of candidates counted across all epochs. The same procedure was applied to candidates marked by BkgStabaDet. Because a candidate can be marked by both popDet and BkgStabaDet, the total percentage of rejected artifacts by popDet and BkgStabaDet can exceed 100.

3. Results

3.1 Minimum event duration does not significantly impact SOZ localization

SOZ localization results were similar when HFO detection was done using minimum event duration (thldt) values of 6ms or 12ms. We noted this pattern in all subjects; one representative example is shown in Figure 3. Comparing the heatmaps in Figures 3A and 3B, the range of optimal F1 scores remains the same across the parameter space, with the highest optimal F1 score achieved using a low threshold and short RMS window. A similar pattern of optimal parameters occurs in the AUC values. Because minimum event duration did not significantly alter localization results for any patient, even when doubling its value, the remaining results will be reported using only a minimum event duration of 6ms.

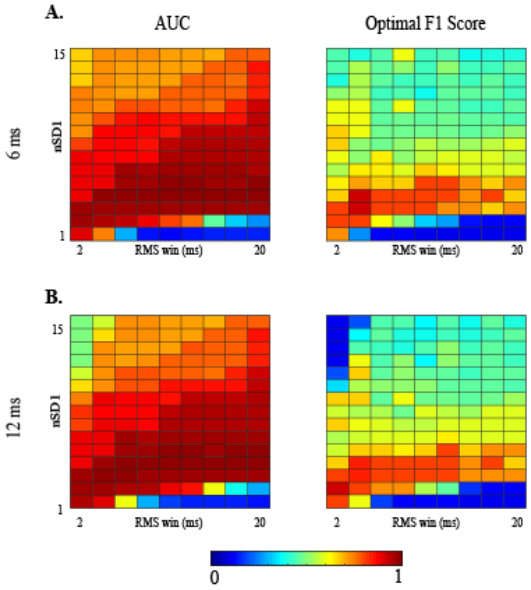

Figure 3. Minimum event duration does not affect SOZ localization performance. SOZ localization performance across the parameter space, comparing results calculated using minimum event duration of (A) 6ms and (B) 12ms. Representative heatmaps of AUC and optimal F1 score are shown across the parameter space for subject 5, with RMS window length (RMS_win) varying on the horizontal axis and RMS threshold (nSD1) varying on the vertical axis. All values range from 0 to 1, with results closer to 1 indicating good classification of SOZ and nSOZ channels.

3.2 Artifact rejection does not significantly impact SOZ localization

Detection with and without artifact rejection generally lead to the same optimal parameters for optimal F1 score and AUC for all patients. A representative example of localization performance before artifact rejection is shown in Figure 4A. For this subject, the best performance, denoted by the highest optimal F1 score, occurs when the threshold is low (around nSD1 3-5) and across most RMS window sizes. Similar results are achieved after artifact rejection (Figure 4B). The optimal parameter set is the same in both cases (RMS_win = 3ms, nSD1 = 4), but we note that artifact rejection does improve performance for higher values of nSD1 for this patient. Across all patients, the optimal parameters were maintained after artifact rejection, with some improvement in other parameter sets.

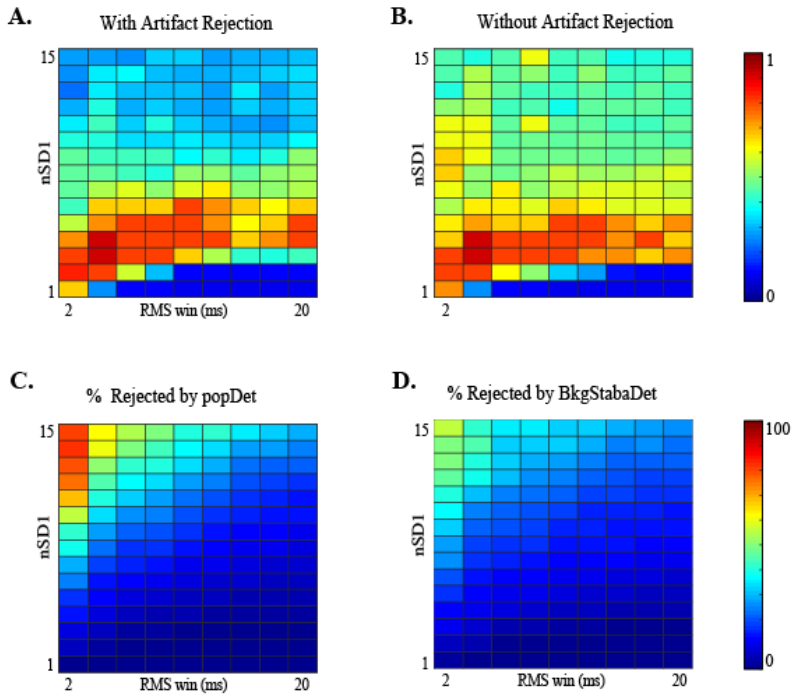

Figure 4. Artifact rejection does not impact the optimal detection parameters. Comparison of optimal F1 scores (A) with and (B) without artifact rejection across the parameter space. Percentage of candidate events rejected by (C) popDet and (D) BkgStabaDet across the parameter space. Results from patient 5 are shown as a representative example.

The percent of rejected artifacts varied across the parameter space (Figure 4C, D). Near the optimal parameter set, the percent of rejected artifacts by the popDet ranges from 5.2 – 8% and by the BkgStabaDet ranges from 6.6 – 9% for this representative example. Generally, higher percentages of detected events were rejected as artifacts when the RMS window was short and the threshold was high (top left corner of Figure 4C, D). In contrast, the smallest percentages of rejected artifacts were found when the RMS window was long and the threshold was low (bottom right). This pattern was similar across all subjects and for both artifact rejection methods. The total percentage of rejected artifacts was also generally consistent across patients.

3.3 Optimal parameters are patient-specific and vary across a wide range

The optimal HFO detection parameters, which are associated with the maximum AUC and optimal F1 score, varied across patients. Figure 5 displays the SOZ localization results for all twenty patients reported as optimal F1 score (left) and AUC (middle). A consistent range of generally good performance can be found for all patients as the RMS window and threshold increase simultaneously (indicated by the red bands stretching from the lower left corner to the upper right corner). However, within this range, patients have their own subrange of optimal parameters. Four of the twenty patients (patient 4, 5, 7, and 17) display a similar pattern with optimal values at or near the default detection parameters. These same patients reported high optimal F1 scores and AUC values, indicating a clear distinction between the SOZ and nSOZ channels based on HFO rate. Four of the twenty patients (patients 2, 3, 8, and 19) had optimal

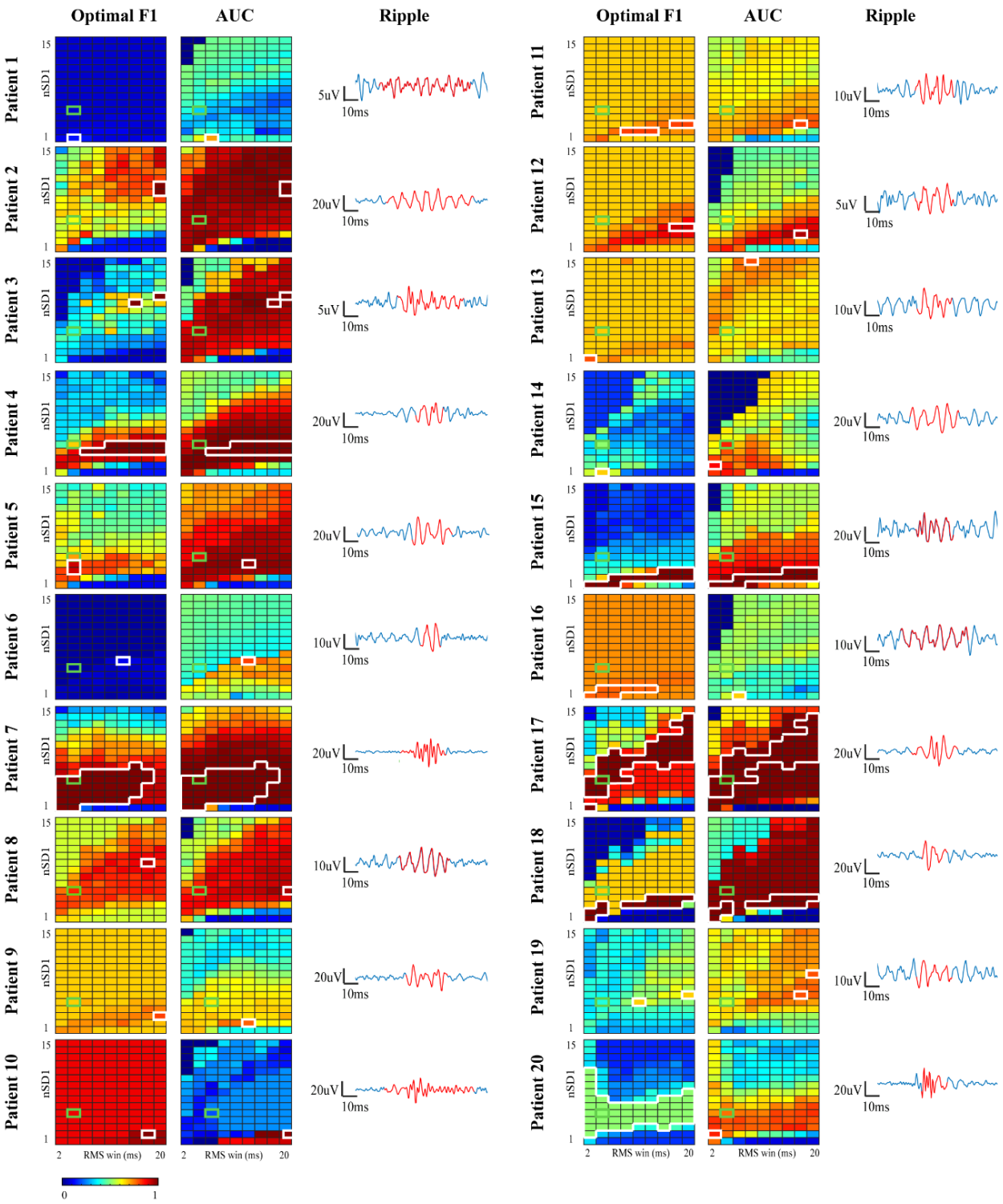

Figure 5. Optimal HFO detection parameters are patient-specific. Optimal F1 scores (left column) and AUC values (middle column) across the parameter space are shown for all patients. Results based on the default detection parameters are outlined in green. Parameter sets achieving optimal SOZ/nSOZ classification are outlined in white. Representative ripples (right column) detected using optimal parameters.

parameters using a stricter threshold and larger RMS window based on the optimal F1 score results. This differed significantly from the default parameters; however, patient 8 obtained similar localization results at the default parameters compared to the optimal parameters. In six patients (patients 4, 7, 15, 16, 17, 18), the optimal parameters were spread over a wide range that included various RMS window lengths, indicating little influence of the RMS window parameter on detection. Five patients (patient 1, 6, 14, 19, and 20) had low optimal F1 scores across the parameter space, suggesting a substantial presence of false positives. However, three of these patients (patient 6, 14, and 20) displayed favorable results based on the ROC curve, indicating that the number of true positives was also high.

3.4 Variability of class imbalance amongst patients affects interpretation of results

For all seven patients from the UCI dataset (patients 1-7), the range of optimal parameters was greater based on ROC results compared to PR results. This can be explained by the definition of precision and false positive rate — two distinct components of the PR and ROC curve. Precision is interpreted as a positive predictive value determined by the number of true positives relative to all predicted positives as defined in equation 3. In patients from the UCI dataset, the number of nSOZ channels considerably outnumbers the SOZ channels; this increases the probability of marking a false positive, which increases the denominator of equation 3. Furthermore, since there are fewer true positive SOZ channels, the probability of obtaining a significant positive predictive value is low due to the large class imbalance. In contrast, the false positive rate in ROC analysis is interpreted as how often the positive class is predicted positive

when the actual outcome is negative, or in other words, the proportion of false positives of the nSOZ channels. Due to the large number of true negative (nSOZ) channels, the false positive rate can generally be kept low while the true positive rate increases, resulting in more favorable ROC results within the UCI dataset.

For example, in patient 6, good classification performance was only visible in the AUC of the ROC curve. In the case of patient 6, we observe that the HFO rate distribution contains a considerable number of nSOZ channels with high HFO rates (Figure 6A). At least five nSOZ channels have higher HFO rates than the SOZ channel, thereby giving a poor PR curve (Figure 6B). However, we see a better ROC result due to the large proportion of nSOZ channels with lower rates compared the SOZ channel (Figure 6C). This case study suggests that nSOZ channels with high HFO rates significantly affect the positive predictive value in PR, but they have a modest effect on ROC analysis when the proportion of nSOZ channels outweighs the SOZ channels.

In contrast to the UCI dataset, most patients from the ETH Zurich dataset (patients 8-20) had wider ranges of optimal parameters based on the PR results (left) compared to the ROC results (right). This relationship is inverted compared to the UCI dataset due to the smaller sampling of analyzed electrodes and broader interpretation of the SOZ, which was defined by the resected area. Therefore, the proportion of SOZ channels outweighs the nSOZ channels, improving the likelihood of obtaining favorable positive predictive performance. Furthermore, due to the decreased number of electrodes, we see less variation in results across the parameter space for some ETH Zurich patients (patients 9, 10, 11, 12, 13, and 16).

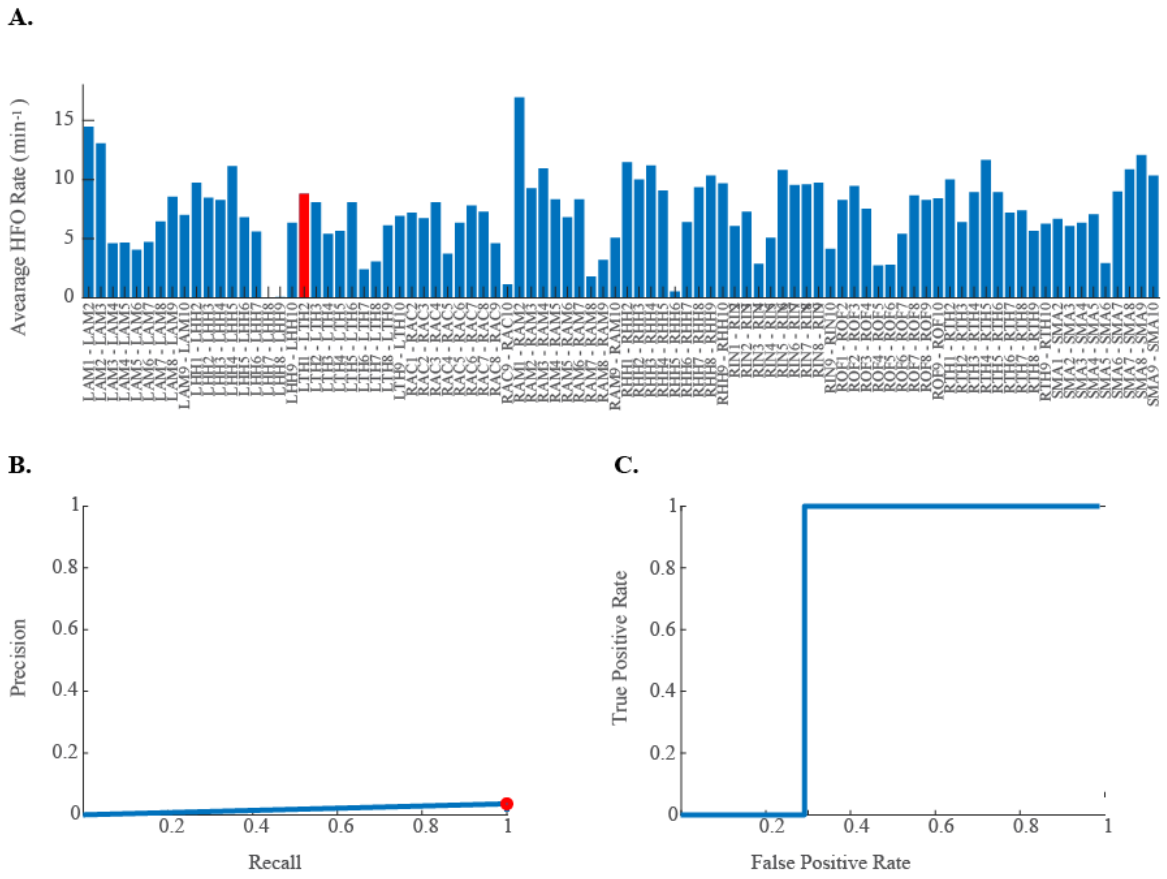

Figure 6. Imbalanced proportion of SOZ channels and nSOZ channels can lead to different interpretations of precision-recall and receiver-operator-characteristic results. (A) Distribution of HFO rates across channels using an RMS threshold of three standard deviations (nSD1=3), RMS window size of 20ms (rms_win=20ms), and minimum event duration of 6ms (thldt=6ms) for patient 6. (B) The resulting PR curve with the optimal F1 point circled in red, and (C) the ROC curve.

3.5 Optimizing HFO detection parameters improves SOZ localization

For each patient, we determined the optimal parameter set based on the highest optimal F1 score and AUC result, then compared the results obtained from these parameters to the default detection parameters (Figure 7). We found substantial increases in optimal F1 scores (>0.2) for eight of the twenty patients (patients 2, 3, 4, 5, 12, 15, 18, 19; Figure 7A). For five of these patients, improvements in the optimal F1 score was primarily driven by an increase in precision, while the remaining three showed improvement influenced by increased sensitivity or

a balance of both measures (Figure 7C). These same patients also showed improved AUC results, with three patients (patients 12, 15, and 18) showing substantial improvement. Two patients (patients 7 and 17) showed no change in optimal F1 score or AUC because the optimal parameters matched the default parameters with good localization accuracy.

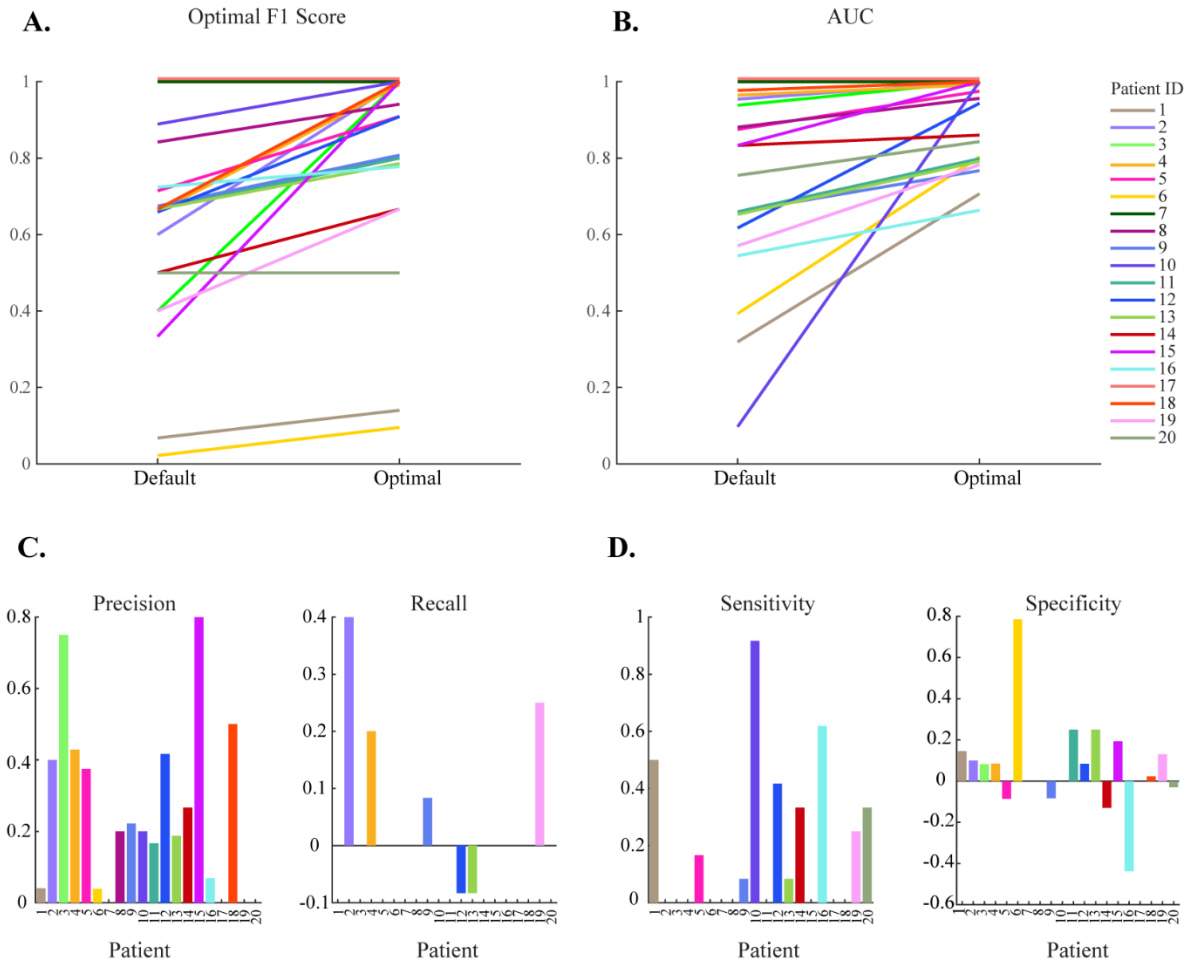

Figure 7. The use of optimal HFO detection parameters improves precision, sensitivity, and specificity. Results for default values vs. optimal values are shown for (A) Optimal F1 scores and (B) AUC results for all patients. (C) Change in Precision and Recall scores (optimal – default). (D) Change in sensitivity and specificity (optimal – default).

Patient 20 also showed no change in the optimal F1 score due to consistent optimal and default parameters, however showed improvement in AUC driven by sensitivity. Six patients (patients 8, 9, 10, 11, 13, and 16) had reasonable localization results (optimal F1 score > 0.6) using default parameters, however still showed improvement in optimal F1 using optimal parameters. The remaining three patients (patients 1, 6 and 14) showed marginal growth in optimal F1 scores, but the value did not exceed 0.65. In the majority of patients, the improvements in optimal F1 score and AUC were due to increases in precision and sensitivity. Outliers from this pattern include patients 6 and 19, which primarily showed improvement as a result of increased recall and specificity. Note that improvements in ROC results carry more weight than improvements in optimal F1 scores because the optimal F1 score represents the best localization possible, while the AUC represents the overall localization accuracy across a range of parameters. In total, seventeen of the twenty patients showed improved localization results using optimized detection parameters, while the remaining three maintained the same results.

3.6 Optimal parameters vary widely across the parameter space

For each patient, we plotted all optimal parameter sets to visually represent the range of optimal detection parameters (Figure 8). The optimal parameters derived from the optimal F1 score (Figure 8A) and AUC (Figure 8B) span the parameter space. Most patients had the same or similar optimal parameters determined from both measures; deviants from this pattern include patients 5, 8, 13, and 20. For many patients, multiple parameter sets produced the same optimal results (i.e. the best result was obtained with more than one parameter set), indicated by multiple points on each plot, and these sets tended to span across RMS window sizes.

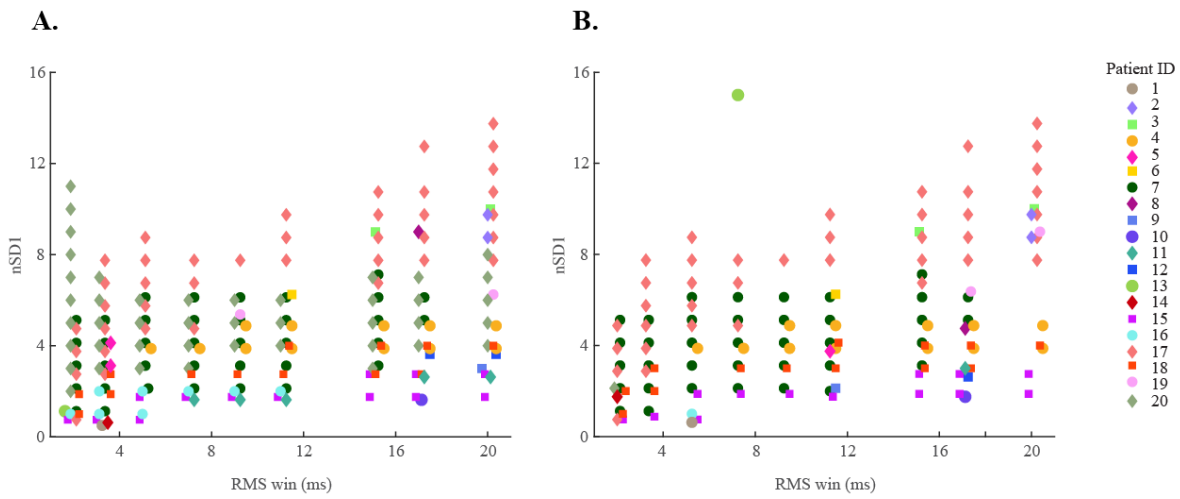

Figure 8. Optimal HFO detection parameters based on (A) optimal F1 score and (B) AUC for all patients.

3.7 Combining HFO rates across various thresholds enables optimal SOZ localization

We have thus far demonstrated the significance of choosing optimal HFO detection parameters by comparing a wide range of values, and this enabled us to determine one or more optimal parameters sets. However, a critical question remains unanswered: how can the optimal parameter set be determined in a patient with unknown SOZ and EZ? To address this question, we propose a method to simplify the optimization procedure. Based on our results from varying detection parameters, we found evidence that supports the notion that HFOs in SOZ channels are dominant over a wide range of parameters (Pail et al., 2013). Considering the characteristics of HFOs, we expect pathological HFOs in the SOZ to exhibit high amplitudes compared to the background (high signal-to-noise ratio), resulting in detection across a range of thresholds. For example, the nSOZ channels may contain less prominent HFOs that may have just barely

exceeded the detection threshold. We therefore hypothesized that we could localize the SOZ by studying the change in average HFO rate while varying the detection threshold.

To test this hypothesis, we localized the SOZ by identifying channels with the highest HFO rates *and* smallest change in rate across varying detection thresholds, rather than identifying SOZ channels solely by the greatest HFO rates. We plotted the average HFO rate as the threshold increased and calculated the area under the curve for each channel for all twenty patients. A large area under the curve indicates that the channel has a persistently high HFO rate over a range of thresholds. Figure 9A shows the log-transformed average HFO rate using an RMS window of 3ms for patient 7 as an example. We found that the average HFO rate of SOZ

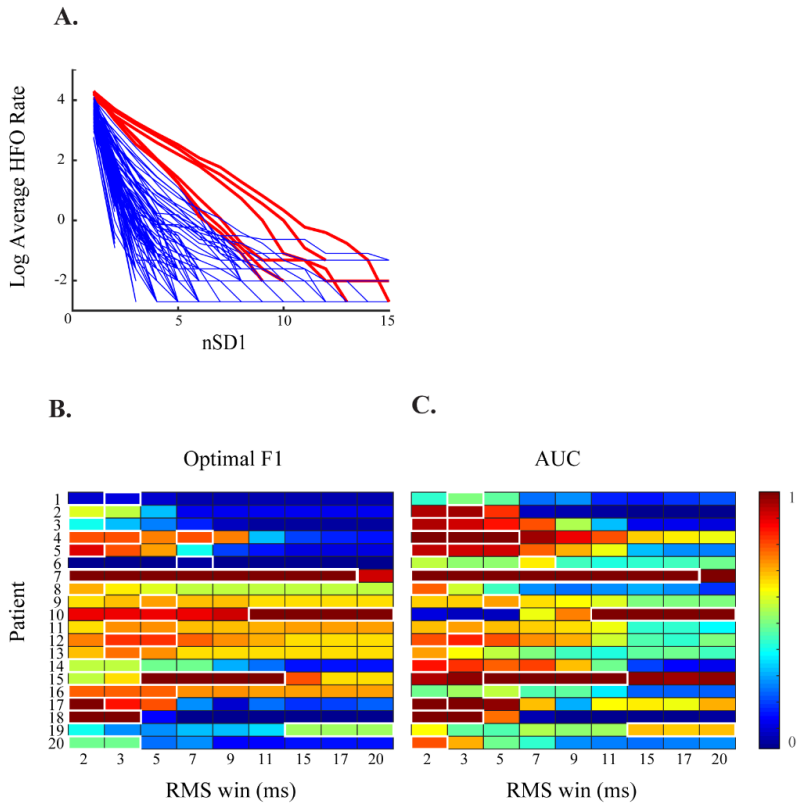

Figure 9. An alternative optimization procedure, based on measurements of HFO rates across varying thresholds, leads to similar SOZ localization accuracy compared to the conventional method. (A) Example of HFO rates as a function of RMS threshold (nSD1) for patient 7 using RMS window length of 3ms. The SOZ channels (red) have higher HFO rates, and this rate decreases slowly as the threshold is increased, leading to a higher area under the curve than nSOZ channels (blue). (B) Optimal F1 Score results for all patients using our alternative optimization procedure with varying RMS window lengths. (C) AUC of ROC result using the alternative optimization procedure. For both optimal F1 score and AUC, good localization results are obtained using short RMS windows.

channels (red) decreased at a slower rate compared to the nSOZ channels (blue) as the threshold increased. We calculated the area-under-the-curve of the average HFO rate for all nine RMS window parameters for each patient. We then applied a threshold to the distribution of area-under-the-curve values across all channels; we classified channels exceeding the threshold as SOZ and the remaining as nSOZ. Following the procedure described previously, we analyzed the classifier performance using the optimal F1 score of the PR curve (Figure 9B) and the AUC of the ROC curve (Figure 9C).

Across all patients, we found similar optimal localization results with the conventional method (HFO rate only) and our alternative method (HFO rate plus change in HFO rate). The classification accuracy was similar for all patients; specifically, patients with good localization results using the conventional method achieved good localization results using this alternative method, and patients with low to average localization results using the conventional method achieved low to average localization results using this alternative method. For eleven patients (patients 1, 4, 7, 11, 12, 13, 14, 15, 16, 18, and 20), the optimal results based on optimal F1 were obtained at an RMS window length of 3ms, and five patients (patients 2, 3, 8, 9, and 10) were within 0.07 of their optimal performance for this window length. Two patients (patients 5 and 17) within 0.15 of their optimal performance reported optimal F1 scores of at least 0.8 at this window, indicating good localization accuracy despite not using the optimal parameters. This outcome is interesting because the optimal results occurred within a consistent range of RMS window values using the alternative method, whereas the optimal RMS window values varied widely using the conventional method. We hypothesize that shorter RMS windows provided better localization results in the alternative method because it results in detection of greater

numbers of candidate HFOs, which leads to more accurate average HFO rates across a range of thresholds.

In summary, we found a possible alternative method to localizing the SOZ which removes the requirement of optimizing detection parameters. In the conventional method, one set of detection parameters is used to generate a distribution of HFO rates across channels. In our proposed alternative method, the HFO rate is measured while the RMS threshold is varied; the area under this curve can be used to classify SOZ and nSOZ channels. Because good results were obtained for short RMS window lengths (implying that this parameter does not need to be optimized), it may be possible to use this method to completely eliminate the need for optimization. However, further analysis and more patient data should be explored to investigate the feasibility and reliability of this method.

4. Discussion

4.1 Summary of findings

This study assessed SOZ localization accuracy over a wide range of HFO detection parameters to study the significance of parameter optimization in two patient cohorts. In both patient populations, we found that the range of parameters for optimal classification of SOZ/nSOZ electrodes was patient-specific, and the most critical parameters were the RMS window length and the thresholds. Additionally, we reported that detection using optimal parameters led to improved localization results compared to the standard parameters given in the original publication. We also suggested an alternative optimization procedure based on the hypothesis that HFOs in SOZ channels are robustly detected over a wide range of parameters. We found that quantifying HFO rate while varying the detection threshold could be used to classify SOZ/nSOZ channels with accuracy similar to the conventional method using HFO rate from a single, optimal parameter set.

4.2 Influence of class imbalance on interpretation of results

In this study, the class imbalance (number of SOZ channels relative to nSOZ channels) greatly affected the interpretation of the results for each patient. The number, type, and placement of electrodes varied per patient based on clinical indication, resulting in inconsistent sample sizes. Furthermore, the localized SOZ was specific to each patient as expected, leading to variable numbers of SOZ channels and nSOZ channels. Because of this, we characterized the classification performance using both the ROC and PR curves, as they are complementary measures. The ROC curve provides valuable information on the classification sensitivity for each

parameter set, and it has been widely used to characterize classification performance. In the UCI dataset, characterized by larger proportions of observed nSOZ channels for all patients, we saw smaller variations in AUC ROC results across the parameter space. This was due to the small proportion of observed SOZ channels, resulting in true positive rates that varied only marginally as the rate threshold was varied. In contrast, the Precision-Recall curves provide valuable information on the positive predictive value of the classification, and this method is considered to be appropriate for analysis in imbalanced datasets (Saito & Rehmsmeier, 2015). Since the positive predictive value is indicative of the proportion of true positives relative to the predicted positives, this metric varies more significantly than the true positive rate (which is used in ROC analysis). Furthermore, the PPV provides key information on the presence of false positives, which occur more frequently in the UCI dataset, as opposed to false negatives, which occur infrequently due to the smaller proportion of SOZ channels. As a demonstration of this, we observed more localized optimal parameter ranges for the optimal F1 scores than the AUC for all UCI patients in Figure 5.

The patterns described here for both ROC and Precision-Recall curves were also observed in the ETH Zurich dataset, albeit reversed since the proportion of observed SOZ channels was greater. Because we cannot compare classification accuracy between the UCI dataset and ETH Zurich dataset directly due to the variables described, we only conclude that the patient's optimal parameters differ, and cannot make comparisons on how well the detector performed across the patient populations. In summary, the dissimilarities in electrode sampling led to different ROC and PR outcomes and for some patients, localization was deemed poor based on these results.

4.3 Characteristics of resulting HFO detections

Detecting HFOs over a wide range of parameters led to substantial differences in the number of HFOs detected. For parameter sets with low thresholds and small RMS windows, we detected more than 1,000 HFOs per channel on average for all patients. These detections are likely a mix of true HFOs and artifacts, and in some cases, the resulting distribution of average detection rates across channels yielded favorable localization results when a rate threshold was applied. In the opposite corner of the parameter space, parameter sets with high thresholds and large RMS windows contained very few detections. These detections are inordinately high amplitude oscillations that must meet the threshold and minimum event duration criteria, especially when the amplitude is damped by the use of a large RMS window. We detected very few of these events, as low as 0-3 detections across all channels, which likely led to the unreliable localization results when using these extreme parameters. The best localization results for patient 2 occurred for some parameter sets in this region, suggesting that identifying high amplitude HFOs may improve SOZ localization. This is consistent with previous findings that demonstrate amplitude as an important metric in HFO analysis (Charupanit et al., 2020; Malinowska et al., 2015; Matsumoto et al., 2013).

4.4 Influence of underlying pathologies

A subset of patients did not achieve accurate SOZ localizations for any parameter set, and to the presence of secondary pathologies or specific epilepsy disorders is one possible explanation for this. In the UCI dataset, MRI results of patients 1, 2, 3, and 6 revealed lesional or tissue abnormalities consisting of hippocampal and temporal sclerosis, cortical dysplasia of the

prefrontal cortex, and imaging abnormalities in the frontal cortex. The presence of these secondary pathologies may have influenced the HFO rates detected in these regions, due to various types of neuronal derangements in abnormal brain tissue (Ferrari-Marinho et al., 2015). Regarding the influence of epilepsy disorder on HFO rate in the SOZ, previous studies have found distinctions between patients with temporal and extratemporal epilepsy. For example, Guragain et al. (2018) examined the spatial mapping of HFOs and found that patients with extratemporal epilepsy disorders did not contain significantly elevated HFOs rates in the SOZ compared to the nSOZ. In contrast, patients with mesial temporal epilepsy showed significantly elevated HFO rates in the SOZ, suggesting that HFOs may be a specific marker for patients with mesial temporal lobe epilepsies (Bragin et al., 1999; Staba et al., 2004; Greg A. Worrell et al., 2008). Similar distinctions were found between patients with neocortical epilepsies and mesial temporal lobe epilepsies, where patients with neocortical epilepsies did not exhibit HFOs in epileptic structures or healthy regions (Crépon et al., 2010). However, HFOs were recorded in the SOZ of all patients with mesial temporal lobe epilepsy (Crépon et al., 2010). Of the UCI patients included in this study, patient 1 was diagnosed with frontal lobe epilepsy, which may explain the suboptimal SOZ localization results across all parameter sets. Similarly, patients 14-20 from the ETH Zurich dataset were diagnosed with extratemporal epilepsy and underwent lesionectomy, which may have influenced localization because different lesion types have various levels of intrinsic epileptogenicity and may contribute dissimilarly to epileptogenic networks (Jacobs et al., 2009). In summary, underlying pathologies may play a role in the ability to accurately localize the SOZ based on findings within our cohort; however additional patients should be studied to make proper conclusions.

4.5 Limitations and future work

There are several limitations to our work. Firstly, we had a limited cohort size. However, our results were consistent across two independent datasets, with each dataset demonstrating patient-specific variability in optimal parameters. This was the main goal of our study. Secondly, although the results for the ETH Zurich dataset support our claim that optimal parameters vary per patient, the delineation of the resected volume, rather than the SOZ, restricted our ability to make more definitive conclusions regarding SOZ localization. For classification purposes, we defined the SOZ as the resected volume, which is typically a larger region of the brain that encompasses the SOZ. Therefore, the SOZ was loosely defined for the ETH Zurich dataset, which most likely affected ROC and PR results.

Regarding automatic HFO detection, we aimed to analyze artifact-free intracranial EEG data during sleep. However, concurrent scalp EEG was not available for the UCI dataset, and the data were therefore not sleep staged. Previous studies have shown that HFO activity varies across wakefulness and sleep and for specific sleep stages (Bagshaw et al., 2009; Clemens et al., 2003; Staba et al., 2004). Therefore, ensuring that all data were recorded during the same sleep stage may provide more accurate results. Another significant limitation in our study was the optimization of our artifact rejection methods. Although Gliske et al. (2016) performed an optimization procedure to determine the rejection threshold of the popDet, one set of parameters does not necessarily work equally well for all patients, as we have shown here. Furthermore, Gliske et al. (2016) tested the threshold ranging from 5 to 15 standard deviations; however, in some of our patients, we found that the popDet performed better using a lower threshold. Ideally, to improve localization results, visual validation should be used to optimize parameters for artifact rejection.

Lastly, our study demonstrates that patient-specific optimization can significantly improve SOZ localization; however, two important questions remain unanswered. First, we must develop methods to implement this per-patient optimization in clinical practice. Our analysis was retrospective, and we reported the best possible localization results assuming that the optimal detection parameters were chosen; however, in clinical practice, optimization would need to be performed on a reserved subset of patient data and without prior knowledge of the SOZ. Thus, future work should address the feasibility of implementing per-patient optimization in clinical settings. Second, we did not address the question of whether the improvement in SOZ localization is clinically meaningful. For example, if the AUC increases from 0.80 to 0.85 due to parameter optimization, would this change the patient's treatment or outcome? What is the minimum level of improvement needed to provide a positive clinical impact? It may be possible to estimate the impact by quantifying the differences in observed true positives and false positives, however this is not trivial, as the consequences for selection (or omission) of individual channels will be specific to each patient. Future work should aim to address the question of what constitutes clinically meaningful improvement.

5. Conclusion

This study examined the impact of optimization of automatic HFO detection parameters on SOZ localization in medically intractable epilepsy patients. All patients achieved seizure freedom following resective surgery, and we found that the majority of patients contained elevated HFO rates in the SOZ, which led to favorable localization results. Only a subset of these patients achieved their maximum localization accuracy using conventional detection parameters, highlighting the significance of patient variability and the importance of tuning automatic HFO detectors. We hypothesized that patients' underlying pathologies may have influenced HFO rates, leading to unconventional optimal parameters, though a larger dataset is needed to definitively test this. We further sought to suggest an alternative HFO detection procedure that has the potential to eliminate the need for parameter optimization. We found that quantifying the change in HFO rate while varying detection thresholds led to similar localization results compared to the conventional method based on HFO rate at a single detection threshold. This suggests that high amplitude HFOs, which are dominant across various thresholds, may be a robust marker of the SOZ. Future studies should examine the characteristics of pathological HFOs, such as amplitude, and continue to explore whether patterns of HFO rate can be used to differentiate epileptic tissue.

6. References

Akiyama, T., McCoy, B., Go, C., Ochi, A., Elliott, I., & Akiyama, M. et al. (2011). Focal resection of fast ripples on extraoperative intracranial EEG improves seizure outcome in pediatric epilepsy. Epilepsia, 52(10), 1802-1811. https://doi.org/10.1111/j.1528-1167.2011.03199.x

Bagshaw, A. P., Jacobs, J., Levan, P., Dubeau, F., & Gotman, J. (2009). Effect of sleep stage on interictal high-frequency oscillations recorded from depth macroelectrodes in patients with focal epilepsy. Epilepsia, 50(4), 617–628. https://doi.org/10.1111/j.1528-1167.2008.01784.x

Bautista, R., Cobbs, M., Spencer, D., & Spencer, S. (1999). Prediction of surgical outcome by interictal epileptiform abnormalities during intracranial EEG monitoring in patients with extrahippocampal. Epilepsia, 40(7), 880-890. https://doi.org/10.1111/j.1528-1157.1999.tb00794.x

Bénar, C. G., Chauvière, L., Bartolomei, F., & Wendling, F. (2010). Pitfalls of high-pass filtering for detecting epileptic oscillations: A technical note on “false” ripples. Clinical Neurophysiology, 121(3), 301–310. https://doi.org/10.1016/j.clinph.2009.10.019

Blanco, J. A., Stead, M., Krieger, A., Viventi, J., Marsh, W. R., Lee, K. H., Worrell, G. A., & Litt, B. (2010). Unsupervised classification of high-frequency oscillations in human neocortical epilepsy and control patients. Journal of Neurophysiology, 104(5), 2900–2912. https://doi.org/10.1152/jn.01082.2009

Bragin, A., Benassi, S. K., Kheiri, F., & Engel, J. (2011). Further evidence that pathologic high-frequency oscillations are bursts of population spikes derived from recordings of identified cells in dentate gyrus. Epilepsia, 52(1), 45–52. https://doi.org/10.1111/j.1528-1167.2010.02896.x

Bragin, A., Engel, J., Wilson, C., Fried, I., & Buzsáki, G. (1999). High-frequency oscillations in human brain. Hippocampus, 9(2), 137-142. https://doi.org/10.1002/(sici)1098-1063(1999)9:2<137::aid-hipo5>3.0.co;2-0

Bragin, A., Wilson, C., Staba, R., Reddick, M., Fried, I., & Engel, J. (2002). Interictal high-frequency oscillations (80-500Hz) in the human epileptic brain: Entorhinal cortex. Annals of Neurology, 52(4), 407-415. https://doi.org/10.1002/ana.10291

Burnos, S., Hilfiker, P., Sürücü, O., Scholkmann, F., Krayenbühl, N., Grunwald, T., & Sarnthein, J. (2014). Human intracranial high frequency oscillations (HFOs) detected by automatic time-frequency analysis. PLoS ONE, 9(4). https://doi.org/10.1371/journal.pone.0094381

Chaibi, S., Lajnef, T., Sakka, Z., Samet, M., & Kachouri, A. (2013). A comparison of methods for detection of high frequency oscillations (HFOs) in human intracerebral EEG recordings.

American Journal of Signal Processing, 2013(2), 25–34. https://doi.org/10.5923/j.ajsp.20130302.02

Charupanit, K., & Lopour, B. A. (2017). A simple statistical method for the automatic detection of ripples in human intracranial EEG. Brain Topography, 30(6), 724–738. https://doi.org/10.1007/s10548-017-0579-6

Charupanit, K, Sen-Gupta, I., Lin, J. J., & Lopour, B. A. (2020). Detection of anomalous high frequency events in human intracranial EEG. Epilepsia Open, epi4.12397. https://doi.org/10.1002/epi4.12397

Clemens, Z., Janszky, J., Szűcs, A., Békésy, M., Clemens, B., & Halász, P. (2003). Interictal epileptic spiking during sleep and wakefulness in mesial temporal lobe epilepsy: A comparative study of scale and foramen ovale elctrodes. Epilepsia, 44(2), 186-192. https://doi.org/10.1046/j.1528-1157.2003.27302.x

Crépon, B., Navarro, V., Hasboun, D., Clemenceau, S., Martinerie, J., Baulac, M., Adam, C., & le Van Quyen, M. (2010). Mapping interictal oscillations greater than 200 Hz recorded with intracranial macroelectrodes in human epilepsy. Brain, 133(1), 33–45. https://doi.org/10.1093/brain/awp277

Dümpelmann, M., Jacobs, J., Kerber, K., & Schulze-Bonhage, A. (2012). Automatic 80-250Hz "ripple" high frequency oscillation detection in invasive subdural grid and strip recordings in epilepsy by a radial basis function neural network. Clinical Neurophysiology, 123(9), 1721–1731. https://doi.org/10.1016/j.clinph.2012.02.072

Edelvik, A., Rydenhag, B., Olsson, I., Flink, R., Kumlien, E., Kallen, K., & Malmgren, K. (2013). Long-term outcomes of epilepsy surgery in Sweden: A national prospective and longitudinal study. Neurology, 81(14), 1244-1251. https://doi.org/10.1212/wnl.0b013e3182a6ca7b

Fedele, T., Burnos, S., Boran, E., Krayenbühl, N., Hilfiker, P., Grunwald, T., & Sarnthein, J. (2017). Resection of high frequency oscillations predicts seizure outcome in the individual patient. Scientific Reports, 7(1). https://doi.org/10.1038/s41598-017-13064-1

Ferrari-Marinho, T., Perucca, P., Mok, K., Olivier, A., Hall, J., Dubeau, F., & Gotman, J. (2015). Pathologic substrates of focal epilepsy influence the generation of high-frequency oscillations. Epilepsia, 56(4), 592–598. https://doi.org/10.1111/epi.12940

Gardner, A. B., Worrell, G. A., Marsh, E., Dlugos, D., & Litt, B. (2007). Human and automated detection of high-frequency oscillations in clinical intracranial EEG recordings. Clinical Neurophysiology, 118(5), 1134–1143. https://doi.org/10.1016/j.clinph.2006.12.019

Gliske, S., Irwin, Z., Davis, K., Sahaya, K., Chestek, C., & Stacey, W. (2016). Universal automated high frequency oscillation detector for real-time, long term EEG. Clinical Neurophysiology, 127(2), 1057-1066. https://doi.org/10.1016/j.clinph.2015.07.016

Guragain, H., Cimbalnik, J., Stead, M., Groppe, D. M., Berry, B. M., Kremen, V., Kenney-Jung, D., Britton, J., Worrell, G. A., & Brinkmann, B. H. (2018). Spatial variation in high-frequency oscillation rates and amplitudes in intracranial EEG. Neurology, 90(8), E639–E646. https://doi.org/10.1212/WNL.0000000000004998

Jacobs, J., Staba, R., Asano, E., Otsubo, H., Wu, J., & Zijlmans, M. et al. (2012). High-frequency oscillations (HFOs) in clinical epilepsy. Progress in Neurobiology, 98(3), 302-315. https://doi.org/10.1016/j.pneurobio.2012.03.001

Jacobs, Julia, Golla, T., Mader, M., Schelter, B., Dümpelmann, M., Korinthenberg, R., & Schulze-Bonhage, A. (2014). Electrical stimulation for cortical mapping reduces the density of high frequency oscillations. Epilepsy Research, 108(10), 1758–1769. https://doi.org/10.1016/j.eplepsyres.2014.09.022

Jacobs, Julia, LeVan, P., Chander, R., Hall, J., Dubeau, F., & Gotman, J. (2008). Interictal high-frequency oscillations (80-500 Hz) are an indicator of seizure onset areas independent of spikes in the human epileptic brain. Epilepsia, 49(11), 1893–1907. https://doi.org/10.1111/j.1528-1167.2008.01656.x

Jacobs, Julia, Levan, P., Chtillon, C. D., Olivier, A., Dubeau, F., & Gotman, J. (2009). High frequency oscillations in intracranial EEGs mark epileptogenicity rather than lesion type. Brain, 132(4), 1022–1037. https://doi.org/10.1093/brain/awn351

Jacobs, Julia, Zijlmans, M., Zelmann, R., Chatillon, C. É., Hall, J., Olivier, A., Dubeau, F., & Gotman, J. (2010). High-frequency electroencephalographic oscillations correlate with outcome of epilepsy surgery. Annals of Neurology, 67(2), 209–220. https://doi.org/10.1002/ana.21847

Kwan, P., & Brodie, M. (2000). Early identification of refractory epilepsy. New England Journal of Medicine, 342(5), 314-319. https://doi.org/10.1056/nejm200002033420503

Malinowska, U., Bergey, G. K., Harezlak, J., & Jouny, C. C. (2015). Identification of seizure onset zone and preictal state based on characteristics of high frequency oscillations. Clinical Neurophysiology, 126(8), 1505–1513. https://doi.org/10.1016/j.clinph.2014.11.007

Matsumoto, A., Brinkmann, B., Matthew Stead, S., Matsumoto, J., Kucewicz, M., & Marsh, W. et al. (2013). Pathological and physiological high-frequency oscillations in focal human epilepsy. Journal of Neurophysiology, 110(8), 1958-1964. https://doi.org/10.1152/jn.00341.2013

Migliorelli, C., Alonso, J. F., Romero, S., Nowak, R., Russi, A., & Mañanas, M. A. (2017). Automated detection of epileptic ripples in MEG using beamformer-based virtual sensors. Journal of Neural Engineering, 14(4). https://doi.org/10.1088/1741-2552/aa684c

Navarrete, M., Pyrzowski, J., Corlier, J., Valderrama, M., & le Van Quyen, M. (2016). Automated detection of high-frequency oscillations in electrophysiological signals: Methodological advances. Journal of Physiology Paris, 110(4), 316–326. https://doi.org/10.1016/j.jphysparis.2017.02.003

Pail, M., Halámek, J., Daniel, P., Kuba, R., Tyrlíková, I., & Chrastina, J. et al. (2013). Intracerebrally recorded high frequency oscillations: Simple visual assessment versus automated detection. Clinical Neurophysiology, 124(10), 1935-1942. https://doi.org/10.1016/j.clinph.2013.03.032

Pearce, A., Wulsin, D., Blanco, J. A., Krieger, A., Litt, B., & Stacey, W. C. (2013). Temporal changes of neocortical high-frequency oscillations in epilepsy. Journal of Neurophysiology, 110(5), 1167–1179. https://doi.org/10.1152/jn.01009.2012

Ramey, W., Martirosyan, N., Lieu, C., Hasham, H., Lemole, G., & Weinand, M. (2013). Current management and surgical outcomes of medically intractable epilepsy. Clinical Neurology and Neurosurgery, 115(12), 2411-2418. https://doi.org/10.1016/j.clineuro.2013.09.035

Roehri, N., Pizzo, F., Lagarde, S., Lambert, I., Nica, A., McGonigal, A., Giusiano, B., Bartolomei, F., & Bénar, C. G. (2018). High-frequency oscillations are not better biomarkers of epileptogenic tissues than spikes. Annals of Neurology, 83(1), 84–97. https://doi.org/10.1002/ana.25124

Rosenow, F., & Lüders, H. (2001). Presurgical evaluation of epilepsy. Brain, 124(9), 1683-1700. https://doi.org/10.1093/brain/124.9.1683

Saito, T., & Rehmsmeier, M. (2015). The precision-recall plot is more informative than the ROC plot when evaluating binary classifiers on imbalanced datasets. PLoS ONE, 10(3). https://doi.org/10.1371/journal.pone.0118432

Schuele, S., & Lüders, H. (2008). Intractable epilepsy: management and therapeutic alternatives. The Lancet Neurology, 7(6), 514-524. https://doi.org/10.1016/s1474-4422 (08)70108-x

Staba, R., & Bragin, A. (2011). High-frequency oscillations and other electrophysiological biomarkers of epilepsy: underlying mechanisms. Biomarkers in Medicine, 5(5), 545-556. https://doi.org/10.2217/bmm.11.72

Staba, R., Wilson, C., Bragin, A., Fried, I., & Engel, J. (2002). Quantitative analysis of high-frequency oscillations (80-500 Hz) recorded in human epileptic hippocampus and entorhinal cortex. Journal of Neurophysiology, 88(4), 1743-1752. https://doi.org/10.1152/jn.2002.88.4.1743

Staba, R. J., Wilson, C. L., Bragin, A., Jhung, D., Fried, I., & Engel, J. (2004). High-frequency oscillations recorded in human medial temporal lobe during sleep. Annals of Neurology, 56(1), 108–115. https://doi.org/10.1002/ana.20164

Westmoreland, B. (1996). Epileptiform electroencephalographic patterns. Mayo Clinic Proceedings, 71(5), 501-511. https://doi.org/10.4065/71.5.501

Worrell, G., Jerbi, K., Kobayashi, K., Lina, J., Zelmann, R., & Le Van Quyen, M. (2012). Recording and analysis techniques for high-frequency oscillations. Progress in Neurobiology, 98(3), 265-278. https://doi.org/10.1016/j.pneurobio.2012.02.006

Worrell, Greg A., Gardner, A. B., Stead, S. M., Hu, S., Goerss, S., Cascino, G. J., Meyer, F. B., Marsh, R., & Litt, B. (2008). High-frequency oscillations in human temporal lobe: Simultaneous microwire and clinical macroelectrode recordings. Brain, 131(4), 928–937. https://doi.org/10.1093/brain/awn006

Wu, J., Sankar, R., Lerner, J., Matsumoto, J., Vinters, H., & Mathern, G. (2010). Removing interictal fast ripples on electrocorticography linked with seizure freedom in children. Neurology, 75(19), 1686-1694. https://doi.org/10.1212/wnl.0b013e3181fc27d0

Wu, M., Wan, T., Ding, M., Wan, X., Du, Y., & She, J. (2018). A new unsupervised detector of high-frequency oscillations in accurate localization of epileptic seizure onset zones. IEEE Transactions on Neural Systems and Rehabilitation Engineering, 26(12), 2280–2289. https://doi.org/10.1109/TNSRE.2018.2877820

Zelmann, R., Mari, F., Jacobs, J., Zijlmans, M., Chander, R., & Gotman, J. (2010). High Frequency Oscillations for human recordings with macroelectrodes. 2010 Annual International Conference of the IEEE Engineering in Medicine and Biology Society, EMBC'10. https://doi.org/10.1109/IEMBS.2010.5627464

Zelmann, R., Mari, F., Jacobs, J., Zijlmans, M., Dubeau, F., & Gotman, J. (2012). A comparison between detectors of high frequency oscillations. Clinical Neurophysiology, 123(1), 106–116. https://doi.org/10.1016/j.clinph.2011.06.006

Zijlmans, M., Jiruska, P., Zelmann, R., Leijten, F. S. S., Jefferys, J. G. R., & Gotman, J. (2012). High-frequency oscillations as a new biomarker in epilepsy. Annals of Neurology, 71(2), 169–178. https://doi.org/10.1002/ana.22548